First spectroscopic study of odd-odd ^{78}Cu

L. G. Pedersen,[1,*] E. Sahin,[1,†] A. Görgen,[1] F. L. Bello Garrote,[1] Y. Tsunoda,[2] T. Otsuka,[3] M. Niikura,[3] S. Nishimura,[4] Z. Xu,[3,5] H. Baba,[4] G. Benzoni,[6] F. Browne,[4,7] A. M. Bruce,[7] S. Ceruti,[6] F. C. L. Crespi,[6,8] R. Daido,[9,4] G. de Angelis,[10] M.-C. Delattre,[11] Zs. Dombradi,[12] P. Doornenbal,[4] Y. Fang,[9,4] S. Franchoo,[11] G. Gey,[4,13] A. Gottardo,[14] T. Isobe,[4] P. R. John,[15] H. S. Jung,[16] I. Kojouharov,[17] T. Kubo,[4] N. Kurz,[17] I. Kuti,[12] Z. Li,[18] G. Lorusso,[4] I. Matea,[11] K. Matsui,[3] D. Mengoni,[15] T. Miyazaki,[3] V. Modamio,[1] S. Momiyama,[3] A. I. Morales,[6,8,19] P. Morfouace,[11] D. R. Napoli,[20] F. Naqvi,[21] H. Nishibata,[9] A. Odahara,[9] R. Orlandi,[22,23] Z. Patel,[4,24] S. Rice,[4,24] H. Sakurai,[3,4] H. Schaffner,[17] L. Sinclair,[4,25] P.-A. Söderström,[4,26] D. Sohler,[12] I. G. Stefan,[11] T. Sumikama,[27] D. Suzuki,[11] R. Taniuchi,[3,25] J. Taprogge,[4,28] Z. Vajta,[4,12] J. J. Valiente-Dobón,[14] H. Watanabe,[29] V. Werner,[21,30] J. Wu,[4,18] A. Yagi,[9,4] M. Yalcinkaya,[31] R. Yokoyama,[2] and K. Yoshinaga[32]

[1]*Department of Physics, University of Oslo, NO-0316 Oslo, Norway*
[2]*Center for Nuclear Study, The University of Tokyo, 7-3-1 Hongo, Bunkyo-ku, Tokyo 113-0033, Japan*
[3]*Department of Physics, the University of Tokyo, Hongo 7-3-1, Bunkyo-ku, 113-0033 Tokyo, Japan*
[4]*RIKEN Nishina Center, 2-1 Hirosawa, Wako, Saitama 351-0198, Japan*
[5]*University of Hong Kong, Hong Kong, China*
[6]*Istituto Nazionale di Fisica Nucleare, Sezione di Milano, Via Celoria 16, I-20133 Milano, Italy*
[7]*School of Computing, Engineering and Mathematics, University of Brighton, Brighton, BN2 4GJ, United Kingdom*
[8]*Dipartimento di Fisica dell'Università degli Studi di Milano, Via Celoria 16, I-20133 Milano, Italy*
[9]*Department of Physics, Osaka University, 1-1 Machikaneyama, Toyonaka, Osaka 560-0043, Japan*
[10]*INFN Laboratori Nazionali di Legnaro, Legnaro (Pd), 35020 Legnaro, Italy*
[11]*Institut de Physique Nucleaire (IPN), IN2P3-CNRS, Universite Paris-Sud 11, F-91406 Orsay Cedex, France*
[12]*Institute for Nuclear Research (Atomki), Debrecen H-4001, Hungary*
[13]*LPSC, Universite Joseph Fourier, CNRS/IN2P3, Institut National Polytechnique de Grenoble, 38026 Grenoble Cedex, France*
[14]*Istituto Nazionale di Fisica Nucleare, Laboratori Nazionali di Legnaro, I-35020 Legnaro, Italy*
[15]*INFN Sezione di Padova and Dipartimento di Fisica, Università di Padova, 35131 Padova, Italy*
[16]*Department of Physics, University of Notre Dame, Notre Dame, Indiana 46556, USA*
[17]*GSI Helmholtzzentrum für Schwerionenforschung GmbH, D-64291 Darmstadt, Germany*
[18]*Department of Physics, Peking University, Beijing 100871, China*
[19]*IFIC, CSIC-Universitat de València, E-46071 València, Spain*
[20]*INFN Laboratori Nazionale di Leganro, Padova, I-35020 Legnaro, Italy*
[21]*Wright Nuclear Structure Laboratory, Yale University, New Haven, Connecticut 06520-8120, USA*
[22]*Instituut voor Kern- en StralingsFysica, K.U. Leuven, B-3001 Heverlee, Belgium*
[23]*Advanced Science Research Center, JAEA, Tokai, Ibaraki 319-1195, Japan*
[24]*Department of Physics, University of Surrey, Guildford GU2 7XH, United Kingdom*
[25]*Department of Physics, University of York, Heslington, York YO10 5DD, United Kingdom*
[26]*Extreme Light Infrastructure-Nuclear Physics (ELI-NP)/Horia Hulubei National Institute for Physics and Nuclear Engineering (IFIN-HH), Str. Reactorului 30, Bucharest-Măgurele 077125, Romania*
[27]*Department of Physics, Tohoku University, 6-3 Aramaki-Aoba, Aoba, Sendai 980-8578, Japan*
[28]*Instituto de Estructura de la Materia, CSIC, E-28006 Madrid, Spain*
[29]*International Research Center for Nuclei and Particles in the Cosmos, Beihang University, Beijing 100191, China*
[30]*Institut für Kernphysik, Technische Universität Darmstadt, Schlossgartenstr. 9, 64289 Darmstadt, Germany*
[31]*Department of Physics, Faculty of Science, Istanbul University, Vezneciler/Fatih, 34134, Istanbul, Turkey*
[32]*Department of Physics, Tokyo University of Science, 2641 Yamazaki, Noda, Chiba 278-8510, Japan*

(Received 6 October 2022; revised 3 January 2023; accepted 9 January 2023; published 3 April 2023)

Nuclei in the vicinity of ^{78}Ni are important benchmarks for nuclear structure, which can reveal changes in the shell structure far from stability. Spectroscopy of the odd-odd isotope ^{78}Cu was performed for the first time in an experiment with the EURICA setup at the Radioactive Isotope Beam Factory at RIKEN Nishina Center. Excited states in the neutron-rich isotope were populated following the β decay of ^{78}Ni produced by in-flight fission and

*l.g.pedersen@fys.uio.no
†eda.sahin@fys.uio.no

separated by the BigRIPS separator. A level scheme based on the analysis of γ-γ coincidences is presented. Tentative spin and parity assignments were made when possible based on the β-decay feeding intensities and γ-decay properties of the excited states. Time correlations between β and γ decay show clear indications of an isomeric state with a half-life of 3.8(4) ms. Large-scale Monte Carlo shell-model calculations were performed using the A3DA-m interaction and a valence space comprising the full fp shell and the $1g_{9/2}$ and $2d_{5/2}$ orbitals for both protons and neutrons. The comparison of the experimental results with the shell-model calculations allows interpreting the excited states in terms of spin multiplets arising from the proton-neutron interaction. The results provide further insight into the evolution of the proton single-particle orbitals as a function of neutron number, and quantitative information about the proton-neutron interaction outside the doubly magic ^{78}Ni core.

DOI: 10.1103/PhysRevC.107.044301

I. INTRODUCTION

One of the fundamental questions in nuclear physics is how nuclear structure changes when moving away from well-known stable nuclei towards exotic nuclei with large proton-neutron asymmetry. Doubly magic nuclei and their neighbors play a crucial role for understanding the mechanisms that affect the energies and ordering of single-particle orbitals and the size of shell gaps [1,2]. The nucleus ^{78}Ni is of particular interest for studies of shell evolution. With 28 protons and 50 neutrons, it has the largest neutron-to-proton ratio of all closed-shell nuclei with traditional magic numbers. The doubly magic character of ^{78}Ni was recently confirmed in a spectroscopic study that identified the first excited 2^+ state at a high excitation energy of 2.6 MeV [3]. Robust shell closures for both $Z = 28$ and $N = 50$ are consistent with β-decay half-lives of nuclei in the region [4] and with the masses of neutron-rich Cu isotopes [5]. Nuclei with few valence particles or holes outside a ^{78}Ni core represent therefore important benchmarks for theoretical models. The nucleus ^{78}Cu with $Z = 29$ and $N = 49$ is ideally suited to obtain information about the proton-neutron interaction outside the ^{78}Ni core. Properties of nuclei in the vicinity of ^{78}Ni, in particular masses and β-decay half-lives but also the occurrence of isomeric states, are furthermore important for modeling the nucleosynthesis in the region of the first r-process abundance peak [6,7].

Earlier experiments in the ^{78}Ni region have seen evidence for an inversion of the proton $\pi 2p_{3/2}$ and $\pi 1f_{5/2}$ orbitals [8,9]. The ordering of the two states becomes inverted in ^{75}Cu, where the ground state was found to have $I^\pi = 5/2^-$ [8], and an isomeric $3/2^-$ state was found at very low excitation energy [10]. The excitation energy of the $3/2^-$ state continues to increase relative to the $5/2^-$ ground state in ^{77}Cu [9] and ^{79}Cu [11], consistent with the crossing of the $\pi 1f_{5/2}$ and $\pi 2p_{3/2}$ orbitals. The change in single-particle energies was explained by the monopole component of the tensor interaction, which is attractive between the $\nu 1g_{9/2}$ and $\pi 1f_{5/2}$ orbitals but repulsive between the $\nu 1g_{9/2}$ and $\pi 2p_{3/2}$ orbitals [12]. In ^{78}Cu, with only one proton and one neutron hole outside the doubly magic core, relatively pure configurations are expected. The ground state and excited states at low excitation energy are expected to be dominated by the negative-parity multiplet arising from the coupling of an odd proton in the $\pi 1f_{5/2}$ orbital with a neutron hole in the $\nu 1g_{9/2}$ orbital.

The easiest way to couple the valence particles to positive-parity states is by neutron excitation from the $\nu 2p_{1/2}$ into the $\nu 1g_{9/2}$ orbital, leaving an unpaired neutron in the $\nu 2p_{1/2}$ orbital. Positive-parity states are expected to be found at higher excitation energy, and those with low spin are expected to be strongly fed in β decay by allowed transitions.

Shell-model calculations for the heavy odd-odd Cu isotopes were performed earlier by Van Roosbroeck *et al.* using schematic δ and quadrupole-quadrupole (QQ) interactions for single proton and neutron shells outside a ^{68}Ni core, as well as using a larger valence space comprising the pf and $1g_{9/2}$ orbitals for both protons and neutrons with a more realistic interaction [13]. The results of the calculations reflected the transition from particle-particle to particle-hole coupling as neutrons fill the $\nu 1g_{9/2}$ orbital, consistent with expectations from the parabolic rule [14].

Monte Carlo shell-model (MCSM) calculations [15] based on a larger valence space outside a ^{40}Ca core with the A3DA-m interaction [16] were able to reproduce detailed spectroscopic data for both ^{77}Cu [9] and ^{79}Cu [11]. Extending the experimental spectroscopic information to heavier odd-odd Cu isotopes is crucial for understanding the interaction between proton particles and neutron holes outside the ^{78}Ni core and to provide additional benchmarks for the MCSM calculations. It was furthermore shown that residual proton-neutron interactions between the pf and sdg shells have implications for calculating electron-capture rates during core collapse supernovae [17].

Before the present experiment, no excited states in ^{78}Cu were known. Its half-life has previously been measured to be 330.7 ± 2.0 ms [4]. Magnetic-dipole and electric-quadrupole moments have been measured for the ground states up to $A = 78$ [18], which found a tentative assignment of (6^-) for ^{78}Cu. The present work provides the first spectroscopic information on the odd-odd isotope ^{78}Cu. Experimental details and the data analysis are described in Secs. II and III, respectively. Results including spectra, level schemes, and spin-parity assignments, are presented in Sec. IV. The results are discussed and compared with MCSM calculations in Sec. V, followed by a summary and conclusions in Sec. VI.

II. EXPERIMENTAL SETUP

The data presented in this article were obtained in experiments carried out at the Radioactive Isotope Beam Factory (RIBF) of the RIKEN Nishina Centre for Accelerator-based Science outside Tokyo, Japan, during two separate beam times as part of the EURICA campaign [19]. A primary beam of

^{238}U was accelerated subsequently by four cyclotrons to an energy of 345 MeV per nucleon with an average intensity of 10 pnA. In-flight fission reactions of the incident ^{238}U projectiles were induced on a ^{9}Be target of 555 mg/cm^2 areal density, which was located at the F0 focal point at the entrance of the BigRIPS fragment separator [20]. The fission fragments were separated in the first stage of the BigRIPS separator by using the $B\rho$-ΔE-$B\rho$ method [21]. Particle identification (PID) was performed in the second stage of the fragment separator by combining information on the time-of-flight through the separator with the magnetic rigidity $B\rho$ and the characteristic energy loss ΔE of the fragments. The ions of interest were further transmitted through the ZeroDegree spectrometer [21] to the focal point F11, where their β decay and subsequent γ-ray emission were detected. A resulting PID plot can be found in Ref. [4]. The settings of the BigRIPS separator were optimized for the transmission of ^{78}Ni and ^{81}Zn, respectively, during the two experiments.

The separated fission fragments were implanted into the wide-range active silicon-strip stopper array for beta and ion detection (WAS3ABi) [22], which consisted of a stack of eight double-sided silicon strip detectors (DSSSDs). Each detector had 60 horizontal and 40 vertical strips of 1 mm pitch, resulting in a total of 2400 pixels of size 1×1 mm^2 per detector. Each detector had a thickness of 1 mm, with 0.5 mm separation in depth between the detectors. To ensure that the ions were stopped in the center of WAS3ABi, a thin Al degrader was located in front of the detectors. The WAS3ABi array was surrounded by the EURICA array of 12 Euroball Cluster detectors. Each Cluster detector consisted of seven HPGe detectors, yielding a total of 84 Ge crystals with an absolute photopeak efficiency of ≈6.5% for 1.3 MeV γ rays. Ion implantation, β decay, and γ decay events were recorded in time-stamped list mode, allowing the correlation of γ-decay events with the β decays of specific fission fragments that were identified in mass and atomic number. More details on the experimental setup can be found in Refs. [19,22].

III. DATA ANALYSIS

As a first step, subsets of data were generated according to the atomic number Z and mass number A of the ions that were identified in BigRIPS and implanted into WAS3ABi. Ion implantation events were correlated in time and position with subsequent β decays. A total of 7.2×10^3 ^{78}Ni ions were implanted, and 3.0×10^3 correlated β-decay events were detected. The β-decay half-life of ^{78}Ni was found to be $T_{1/2} = 122.2(51)$ ms in a separate analysis of the same data [4], while the Q_β value is 9910 (400) keV [23]. Finally, γ rays detected in the Ge detectors were correlated in time with β-decay events in the Si detectors. The data from the two experiments were analyzed separately, and the resulting γ-ray spectra and γ-γ coincidence matrices were combined afterwards. The individual steps of the data analysis are described in more detail in the following.

Signals from heavy-ion implantation in the DSSSDs are easily distinguished from the detection of β-decay electrons by their signal amplitude. For each implantation event of a ^{78}Ni ion, the data were scanned for the subsequent β decays within a given time window of 2 s. If more than one β-decay event were registered within the correlation time window, only the first one was considered. To reduce the number of random coincidences between implantation and β-decay events, it was required that the implanted ion and β-decay electron were detected in the same, a neighboring, or next to neighboring pixel of the same DSSSD layer.

Finally, correlated events between implanted ions and β decays were used to select γ rays that were promptly following the β decay of ^{78}Ni, within a time window of approximately 200 ns. The information on the time difference between β decays and detected γ rays was furthermore used to search for isomeric decays. In the case that two neighboring crystals within the same Ge cluster detector gave coincident signals, their energies were summed to account for Compton scattering and to increase the detection efficiency for γ rays with high energy.

γ-ray singles spectra were sorted for different correlation time windows between the ion implantation and β-decay events. Because the detection efficiency for electrons in the DSSSD is less than 100%, the β decay can remain undetected. In case a subsequent β decay (or β-delayed neutron decay) occurs within the correlation time window, γ rays from the decay daughter or even granddaughter can appear in the spectrum. Limiting the correlation time to short intervals of the order of the half-life of ^{78}Ni strongly suppresses γ rays originating from subsequent decays but also removes γ rays occurring within ^{78}Cu. The relative suppression of γ rays as a function of correlation time was used to assign unknown γ rays to ^{78}Cu. Known γ rays following the decay of ^{78}Cu into ^{78}Zn, [13] were used to validate the procedure. After the assignment of the strongest γ rays to ^{78}Cu, the strict time constraint between implantation and β decay was relaxed to search for γ-γ coincidences and to construct the level scheme in a compromise between high statistics for the γ rays of interest and suppressing γ rays from daughter decays.

Figure 1 shows a γ-ray singles spectrum for ^{78}Cu. To maximize the level of statistics, a relatively long correlation time window of 2 s was used, resulting in stronger contributions from the daughter decays in ^{77,78}Zn. All peaks that are labeled by their energy were assigned to ^{78}Cu. Some transitions, however, could not be placed in the level scheme because of lacking γ-γ coincidence relationships. These transitions, which are labeled by their energies in parentheses, were assigned to ^{78}Cu based only on their time correlation with the β-decay detection. Where possible, coincidence relationships between γ rays were used to validate their assignment to ^{78}Cu. Examples for gated coincidence spectra are shown in Fig. 2. Only γ rays that could be placed unambiguously were included in the level scheme.

The absolute intensity of β-decay feeding was determined from the intensity balance of γ rays feeding and depopulating a given state, which was corrected for detection efficiency and internal conversion and normalized to the number of implanted ions. However, because of the incomplete level scheme and missing γ-ray feeding from above, this apparent β feeding is only a limit, and a conversion into logft values is not meaningful. The probability for β-delayed neutron emission was measured to be $P_n = 25.8(38)\%$ [24]. The observed

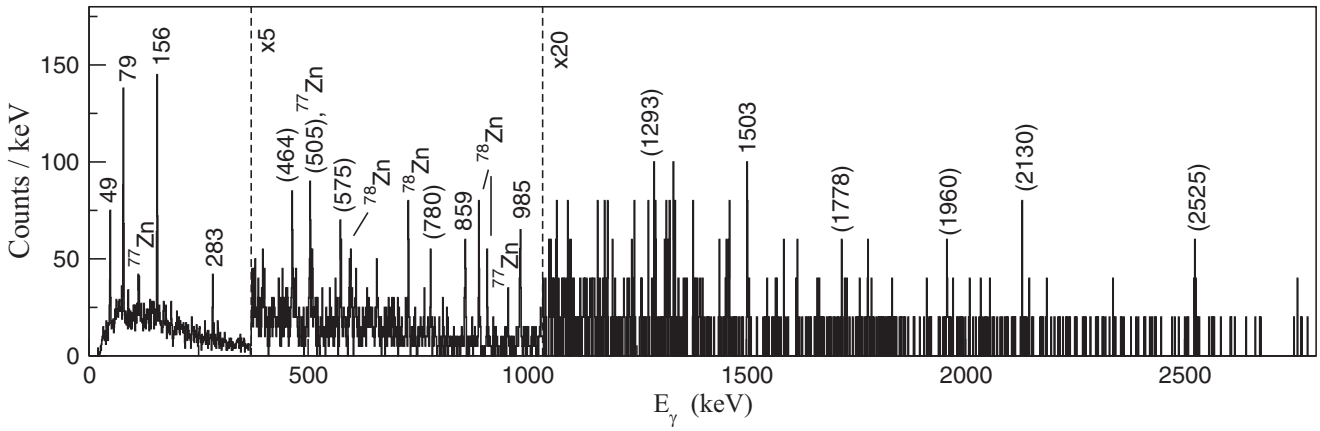

FIG. 1. γ-ray singles spectrum for ^{78}Cu. Note that the higher-energy regions of the spectrum were scaled by the indicated factors. An ion-β correlation window of 2 s was used. Peaks marked by their energy (in keV) are transitions assigned to ^{78}Cu. Energies are given in parentheses for transitions that were assigned to ^{78}Cu but could not be placed in the level scheme. Transitions following the subsequent β and β-n decay of ^{78}Cu are labeled as ^{78}Zn and ^{77}Zn, respectively. The 505 keV transition appears in both ^{78}Cu and the β-n daughter ^{77}Zn.

apparent β feeding accounts for less than 58% of the decays of implanted ions. Taking into account P_n, less than 78% of β-decay feeding was observed. The values for the total observed feeding represents only upper limits and a significant fraction of feeding strength could therefore remain unobserved.

IV. RESULTS

The decay scheme for ^{78}Cu is shown in Fig. 3. The information presented in the decay scheme is furthermore summarized in Table I, together with information on γ-ray intensities and uncertainties for all quantities. It should be noted that no excited states were known prior to the present experiment. The analysis of time correlations allowed associating 16γ-ray transitions with ^{78}Cu, as indicated in Fig. 1. Of these, seven could be placed in the decay scheme based on their coincidence relationships.

The ground-state spin of ^{78}Cu was previously assigned as $(4, 5)^-$ [13] based on the feeding of states in the β-decay daughter ^{78}Zn, and, in later works, as (6^-) [25] and (5^-) [26]. A laser spectroscopy experiment showed best agreement with $I = 6$, suggesting a ground-state spin-parity of (6^-) [18].

The three strongest transitions, with energies of 49, 79, and 156 keV are in mutual coincidence, as shown in Fig. 2. Because they are much stronger than any other transition, it is reasonable to assume that they form a cascade built on the ground state. It can be furthermore assumed that the low-energy transitions connect members of the negative-parity $\pi 1f_{5/2} \times \nu 1g_{9/2}^{-1}$ multiplet, because other configurations are only expected at higher excitation energy. The intensities

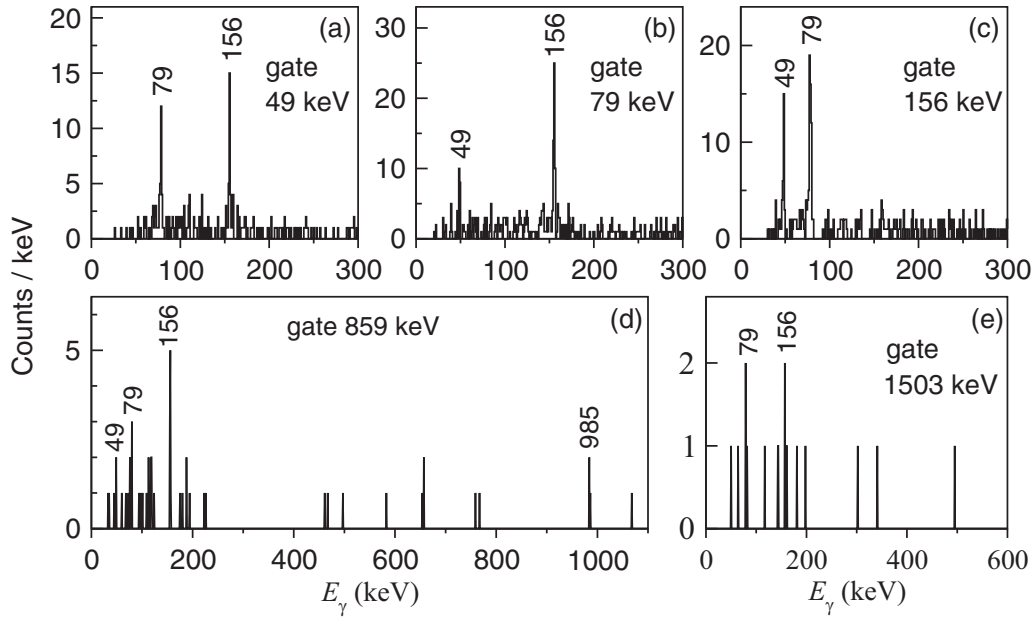

FIG. 2. γ-γ coincidence spectra for ^{78}Cu gated on the (a) 49 keV, (b) 79 keV, (c) 156 keV, (d) 859 keV, and (e) 1503 keV transition.

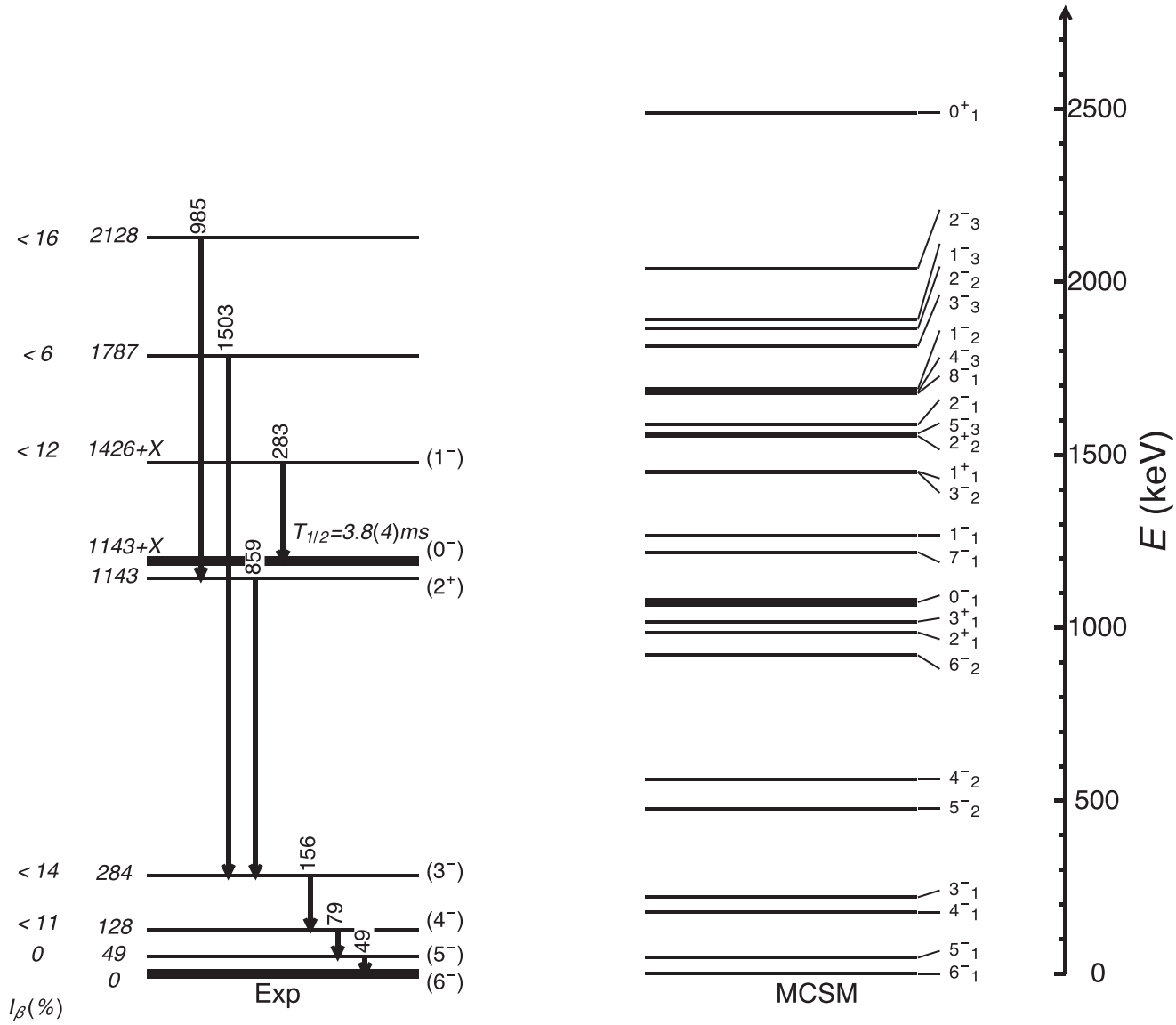

FIG. 3. Experimental level scheme for ^{78}Cu and comparison to MCSM calculations (see text for details).

of the three transitions are approximately the same when taking electron conversion into account and assuming $M1$ multipolarity. Other multipolarities for transitions between negative-parity states would result in significantly higher conversion coefficients. As an example, the conversion coefficient for a 49 keV transition of $M1$ multipolarity is 0.385, whereas it is 8.98 for $E2$ multipolarity [27]. Other multipolarities than $M1$ would therefore either require strong β feeding, which would be highly forbidden, or strong γ feeding that is only in coincidence with one or two transitions within the cascade, for which there is no evidence in the data. Higher multipolarity for transitions with such low energy would in addition result in relatively long lifetimes and delayed coincidences, whereas all three transitions are in prompt coincidence. It can therefore be concluded that the three strongest transitions form a cascade of $M1$ transitions feeding a (6^-) ground state from a (3^-) state at 284 keV. However, the data do not provide any indication for the ordering of the three transitions. According to the empiric rule established by Paar [14], the energies in proton-neutron multiplets with particle-hole character are expected to follow a parabolic trend with $I(I+1)$ and a minimum at spin $I = j_\pi + j_\nu - 1$, which is equal to six in the case of the $\pi 1f_{5/2} \times \nu 1g_{9/2}^{-1}$ configuration. With the ordering of the three transitions within the cascade as shown in the level scheme of Fig. 3, the states fit the expected parabolic trend well, which seems to justify this choice.

The singles spectrum in Fig. 1 shows a transition of 283 keV, and one would be tempted to place this transition as the decay from the 284 keV state. However, the 283 keV transition is not in coincidence with any of the transitions feeding the 284 keV state, as can be seen in Figs. 2(d) and 2(e). Furthermore, the transition would have $M3$ multipolarity if it was depopulating the 3^- state and would therefore unlikely be prompt. Any other ordering of spins for the low-energy states that would allow a prompt 283 keV transition would be in conflict with the observed intensities for the low-energy

TABLE I. γ-ray energies and intensities, along with their initial-state excitation energies, spin and parity, and β feeding.

E_γ (keV)	I_γ (%)	E_i	I^π	β feeding (%)
X		$1143 + X$	$(0v^-)$	
49(1)	43(4)[a]	49(1)	(5^-)	0
79(1)	44(1)[a]	128(2)	(4^-)	<11
156.1(2)	33(1)[a]	284(2)	(3^-)	<14
282.6(7)	12(1)	$1425.7 + X$	(1^-)	<12
464.5(5)	12(1)			
505(2)	9(1)			
575(3)	10(1)			
779.9(6)	7(1)			
859.0(6)	13(1)	1143(2)	(2^+)	
984.5(6)	16(1)	2128(2)		<16
1293(3)	2(2)			
1503(4)	6(2)	1787(4)		<6
1778(4)	3(2)			
1960(2)	2(1)			
2130(3)	2(1)			
2525(3)	2(1)			

[a]Corrected for internal conversion assuming pure $M1$ character.

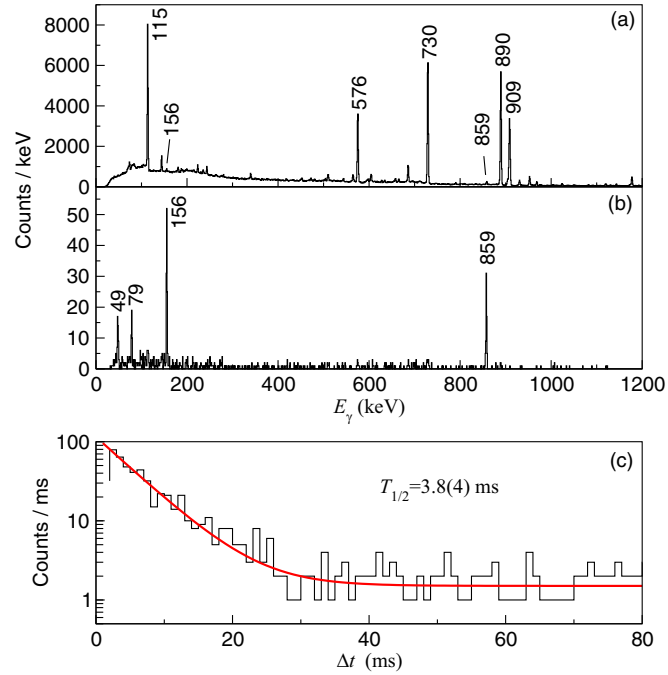

FIG. 4. (a) Decay spectrum of ^{78}Cu ions within 200 ms from implantation in the DSSSDs, revealing known transitions in ^{78}Zn and the 115 keV transition in ^{77}Zn. The small peaks at 156 and 859 keV, originating from excited states in ^{78}Cu, indicate the presence of an isomeric state. (b) Decay spectrum of ^{78}Cu within 5 ms, with an additional condition that a low-energy signal was detected in the same DSSSD pixel as the ion implantation. (c) Time difference between implantation of ^{78}Cu ions and detection of low-energy signals in the DSSSD, with an additional condition that one of the four γ-ray transitions following the decay of the isomer [as seen in spectrum (b)] was detected in EURICA. The exponential fit yields a half-life of $T_{1/2} = 3.8(4)$ ms.

transitions. It is therefore concluded that the 283 keV transition is originating from a state at higher excitation energy.

The 859, 985, and 1503 keV transitions were clearly seen in the γ-ray singles spectrum (see Fig. 1). Based on their time correlations with β decay, they can be identified as belonging to ^{78}Cu. All three transitions are in coincidence with the cascade of three low-energy transitions, as can be seen in Fig. 2. In addition, the 859 and 985 keV transitions are in mutual coincidence. Consequently, the 859 and 1503 keV transitions are placed on top of the (3^-) state at 284 keV excitation energy, and the 985 keV transition on top of the 859 keV transition, feeding a state at 1143 keV excitation energy. With only few transitions placed in the level scheme, the observed β feeding is incomplete and cannot be used for spin assignments. Because the higher-lying states are less likely to be affected by unobserved γ feeding, they are likely to have low spin. The proposed decay scheme is therefore consistent with bridging the large spin gap between states that are fed by allowed β transitions and a (6^-) ground state.

The analysis of time correlations in the decay of ^{78}Cu revealed clear evidence for an isomeric state, as is illustrated in Fig. 4. The spectrum in Fig. 4(a) shows γ rays following the implantation of ions identified as ^{78}Cu [$T_{1/2} = 330.7(20)$ ms] within 200 ms. As expected, the spectrum shows the known transitions in ^{78}Zn and ^{77}Zn [26]. The spectrum also shows hints of the 156 and 859 keV transitions originating from excited states in ^{78}Cu. When selecting a short correlation time of 5 ms, as shown in Fig. 4(b), the cascade of low-energy transitions and the 859 keV transition of ^{78}Cu appears in the spectrum. The spectrum of Fig. 4(b) was further cleaned by selecting events where a low-energy signal was detected in the same DSSSD pixel as the ion implantation, reducing the efficiency for β-decay events and enhancing events originating from conversion electrons. The delayed γ-ray spectrum shows the 859 keV transition, but not the one at 985 keV. This confirms the ordering of the cascade, and clearly shows that the isomeric state is located above the state at 1143 keV. The absence of the 283 keV transition in the delayed spectrum furthermore confirms that it does not originate from the (3^-) state. Because the 283 keV transition is relatively strong, but not seen in coincidence with any other transition, it seems likely that it is feeding the isomeric state.

The time spectrum of the isomeric decay is shown in Fig. 4(c), from which a half-life of $T_{1/2} = 3.8(4)$ ms can be extracted. The spectrum shows the time difference between the implantation of a ^{78}Cu ion and the detection of a low-energy signal in the same pixel of the DSSSD, with an additional condition that one of the four γ-ray transitions following the decay of the isomer was detected. The fact that the decay from the isomer to the state at 1143 keV remained unobserved could be explained by a small energy difference and consequently a large conversion coefficient, consistent with the conversion-electron signal observed in the DSSSD.

Any spin assignment with $I \geqslant 1$ for the isomer would be incompatible with the observed half-life of 3.8(4) ms. For a 1^+ state, for example, a $M2$ transition of at least 859 keV to the (3^-) state would likely result in a half-life of nanoseconds rather than milliseconds. A 1^- assignment or any higher spin would result in prompt decay to one of the low-lying states.

TABLE II. Occupation of proton and neutron orbitals in $fpg_{9/2}d_{5/2}$ spaces.

E (MeV)	J^π	$\pi 1f_{7/2}$	$\pi 2p_{3/2}$	$\pi 1f_{5/2}$	$\pi 2p_{1/2}$	$\pi 1g_{9/2}$	$\pi 1d_{5/2}$	$\nu 1f_{7/2}$	$\nu 2p_{3/2}$	$\nu 1f_{5/2}$	$\nu 2p_{1/2}$	$\nu 1g_{9/2}$	$\nu 1d_{5/2}$
0.000	6^-	7.73	0.25	0.96	0.02	0.04	0.01	7.99	3.99	5.99	1.99	8.86	0.19
0.046	5^-	7.71	0.33	0.87	0.03	0.04	0.01	7.99	3.99	5.99	1.99	8.85	0.20
0.178	4^-	7.71	0.35	0.84	0.05	0.04	0.01	7.99	3.99	5.99	1.98	8.83	0.21
0.221	3^-	7.74	0.46	0.73	0.02	0.04	0.01	7.99	3.99	5.99	1.99	8.86	0.18
0.477	5^-	7.70	0.87	0.30	0.07	0.04	0.01	7.99	3.99	5.99	1.98	8.84	0.21
0.562	4^-	7.74	0.84	0.34	0.03	0.04	0.01	7.99	3.99	5.99	1.98	8.85	0.19
0.921	6^-	7.71	0.95	0.25	0.03	0.05	0.01	7.99	3.98	5.99	1.98	8.88	0.18
0.987	2^+	7.63	0.26	1.04	0.02	0.04	0.01	7.99	3.92	5.92	1.15	9.78	0.24
1.018	3^+	7.60	0.26	1.07	0.02	0.04	0.01	7.99	3.95	5.88	1.15	9.76	0.26
1.074	0^-	7.58	0.29	1.03	0.05	0.04	0.01	7.98	3.92	5.92	1.89	8.13	1.15

Also a 0^+ assignment seems highly unlikely for the isomeric state. An $E3$ transition of at least 859 keV and a strength of 1 Weisskopf unit would result in a half-life of less than 10 μs, 500 times shorter than the observed value. The most likely assignment for the isomeric state is therefore 0^-. A possible $M3$ decay to the state at 284 keV would be sufficiently hindered for it to be unobserved. Instead, a low-energy decay to the state at 1143 keV would become competitive, consistent with the conversion electron signal in the DSSSD. The state at 1143 keV would in this case most likely have spin-parity $I^\pi = 2^+$. The half-life of 3.8(4) ms can be explained by an energy difference of ≈50 keV between the two states and a $M2$ transition of 1 Weisskopf unit. Such a transition would have a conversion coefficient of ≈6, consistent with the DSSSD signal and the nonobservation of a γ ray. Although it is not possible to determine the precise excitation energy of the isomeric state in this way, a 0^- assignment and a low-energy $M2$ transition of a few tens of keV to a 2^+ state at 1143 keV is the only scenario that can explain all observations.

The data are insufficient to determine whether the isomeric state is directly fed by β decay. It is likely that some of the prompt γ-ray transitions that were observed in the singles spectrum for ^{78}Cu feed the isomer. The fact that prompt coincidence relationships are lacking for the relatively strong 283 keV transition suggests that this transition is feeding the isomeric state directly. The resulting state has an excitation energy of $(1427 + X)$ keV, with X being the energy difference between the isomer and the state at 1143 keV.

V. DISCUSSION

To understand the nature of the experimentally observed states, shell-model calculations are necessary. In the present work, we compare the experimental results with Monte Carlo shell-model (MCSM) calculations [15] using the A3DA-m effective interaction, which has successfully described the structure of nuclei in the ^{78}Ni region [9,11,16,28]. The valence space comprised the full pf shell together with the $1g_{9/2}$ and $2d_{5/2}$ orbitals for both protons and neutrons without restrictions. Calculated states up to an excitation energy of 2.5 MeV, for both negative and positive parity, are compared with the experimental level scheme in Fig. 3. Table II shows the occupation numbers for protons and neutrons found in the MCSM calculations for the ten lowest states.

The calculations reproduce the sequence of negative-parity states that was established by the cascade of $M1$ transitions very well, including $I^\pi = 6^-$ for the ground state. The occupation numbers illustrate that these states have a relatively pure particle-hole character based on the $\pi 1f_{5/2} \times \nu 1g_{9/2}^{-1}$ configuration. This is consistent with the inversion of the $\pi 1f_{5/2}$ and $\pi 2p_{3/2}$ orbitals near $N = 48$, which was observed previously [9]. The calculations predict the remaining 2_1^- and 7_1^- members of the multiplet to be at much higher excitation energy, with the negative-parity states based on the $\pi 2p_{3/2} \times \nu 1g_{9/2}^{-1}$ configuration in between. The latter comprises the 5_2^-, 4_2^-, 6_2^-, and 3_2^- states.

The MCSM calculations predict a 0^- state at 1074 keV, close to the excitation energy of the observed isomeric state, which lends further support to the (0^-) assignment for the isomer. The calculations find a relatively pure $\pi 1f_{5/2}\nu 2d_{5/2}$ configuration for the 0^- state. The excitation energy of the isomeric state contains therefore not only information on the interaction energy between the $\pi 1f_{5/2}$ and $\nu 2d_{5/2}$ orbitals, but also on the size of the $N = 50$ shell gap. The good agreement between the experimental and theoretical excitation energy indicates that both quantities are well described by the A3DA-m interaction. The $\pi 1f_{5/2}\nu 2d_{5/2}$ configuration gives rise to a multiplet of negative-parity states comprising the 0_1^-, 1_1^-, 5_3^-, 4_3^-, 3_3^-, and 2_2^- states. The experimental state at $1427 + X$ keV excitation energy is a potential candidate for the 1_1^- state, as strong $M1$ transitions are expected between the states of the multiplet, although such an assignment remains speculative.

All calculated low-lying positive-parity states are based on a neutron excitation from the $\nu 2p_{1/2}$ to the $\nu 1g_{9/2}$ orbital. The coupling between an odd neutron in the $\nu 2p_{1/2}$ orbital and an odd proton in the $\pi 1f_{5/2}$ orbital results in a doublet of the 2^+ and 3^+ states. The occupation numbers of Table II show that the 2_1^+ and 3_1^+ states are indeed dominated by the $\pi 1f_{5/2}\nu 2p_{1/2}$ configuration. The experimental state at 1143 keV, which is tentatively assigned as (2^+), agrees reasonably well with the calculated 2_1^+ state at 987 keV and is consequently a candidate for a member of the $\pi 1f_{5/2}\nu 2p_{1/2}$ doublet. The coupling of a $\nu 2p_{1/2}$ neutron with a $\pi 2p_{3/2}$ proton results in a doublet of the 1_1^+ and 2_2^+ states, which are calculated to be at higher energy around 1.5 MeV. The calculated 0_1^+ state at approximately 2.5 MeV, finally, is found to be based on the $\pi 2p_{1/2}\nu 2p_{1/2}$ configuration. It would be

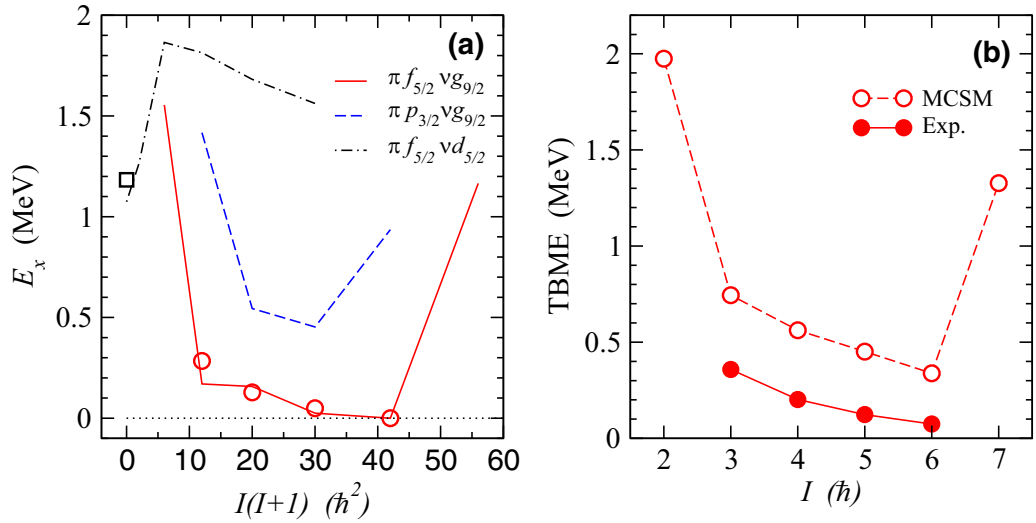

FIG. 5. (a) Excitation energies of the negative-parity multiplets with predominant $\pi 1f_{5/2}\nu 1g_{9/2}^{-1}$, $\pi 2p_{3/2}\nu 1g_{9/2}^{-1}$, and $\pi 1f_{5/2}\nu 2d_{5/2}$ configurations from the MCSM calculations as a function of $I(I+1)$. The symbols indicate the experimental excitation energies for those states for which a tentative spin assignment and association with the multiplet was possible. (b) Two-body matrix elements (TBME) extracted for the $\pi f_{5/2}\nu g_{9/2}^{-1}$ spin multiplet from both the experimental and calculated excited states (see text for details).

speculative to associate any of the higher-lying experimental states with any of the calculated states.

Figure 5(a) shows the excitation energies of the negative-parity states from the MCSM calculations as a function of the squared angular momentum $I(I+1)$. The calculated occupation numbers were used to assign the states to the multiplets with predominant $\pi 1f_{5/2}\nu 1g_{9/2}^{-1}$, $\pi 2p_{3/2}\nu 1g_{9/2}^{-1}$, and $\pi 1f_{5/2}\nu 2d_{5/2}$ configuration. Experimental excitation energies of states with a tentative spin assignment are also included in Fig. 5(a), which illustrates again the rather good agreement between the MCSM calculations and experiment. The multiplets involving a hole in the $\nu 1g_{9/2}$ orbital show a parabolic dependence on angular momentum, with the extreme couplings $I = j_\nu \pm j_\pi$ having the highest energy, as expected for particle-hole coupling [14]. The $\pi 1f_{5/2}\nu 2d_{5/2}$ multiplet, on the other hand, has particle-particle character, which favors (anti-)parallel coupling.

The observed excited states in the odd-odd Cu nuclei allow determining the proton-neutron monopole interaction, which is responsible for changes in single-particle energies, i.e., for the shell evolution far from stability. A description of the procedure to extract two-body matrix elements (TBMEs) from experimental excitation energies of proton-neutron multiplets can be found in Ref. [1]. In the following we apply this procedure for the case of ^{78}Cu. As can be seen in Table II, the negative-parity states of the $\pi 1f_{5/2}\nu 1g_{9/2}^{-1}$ multiplet have relatively pure single-particle (hole) configurations. The results are therefore well suited to extract experimental TBME for the interaction between a $1f_{5/2}$ proton with a $1g_{9/2}^{-1}$ neutron hole. Starting from a ^{78}Ni core, the contributions of a noninteracting proton particle and neutron hole are obtained from the binding energies of ^{79}Cu [5] and ^{77}Ni [23] for the $1f_{5/2}$ proton and the $1g_{9/2}$ neutron hole, respectively. The resulting value is found to be 74 keV lower than the experimental binding energy for the ground state of ^{78}Cu [29], which includes the repulsive residual interaction between the $1f_{5/2}$ proton and the $1g_{9/2}$ neutron hole when coupled to spin 6^-. The TBME for the various spin couplings are consequently shifted by 74 keV compared with the excitation energies of the corresponding states. It should be noted that the masses of ^{77}Ni and ^{78}Ni are not known experimentally, and that the extrapolated values have an uncertainty of 400 keV [23]. The absolute values of the experimental TBME depend therefore strongly on the extrapolated masses of the Ni isotopes. The experimental values are compared with TBME of the A3DA-m interaction in Fig. 5(b), where the theoretical TBME for the $\pi f_{5/2}\nu g_{9/2}^{-1}$ particle-hole interaction were obtained by applying the Pandya transformation [30] to the corresponding particle-particle TBME. The comparison shows that the A3DA-m interaction describes the relative size of the TBME well. The experimental results on the excited states in ^{78}Cu can be used to refine the shell-model interaction once more precise mass values for ^{77}Ni and ^{78}Ni become available.

VI. SUMMARY AND CONCLUSIONS

Excited states in ^{78}Cu have been observed for the first time following the β decay of ^{78}Ni. The neutron-rich ^{78}Ni isotopes were produced at the Radioactive Isotope Beam Factory at RIKEN Nishina Center, Japan, by in-flight fission induced by a primary beam of ^{238}U at 345 MeV per nucleon incident on a ^{9}Be target. The secondary beams were separated by the BigRIPS separator and transported to the decay station, where they were implanted into the WAS3ABi detector. The HPGe detectors of the EURICA array were used to detect γ rays following the β decay of ^{78}Ni. An isomeric state with a half-life of 3.8(4) ms was discovered in ^{78}Cu and tentatively assigned as (0^-). The combination of information from $\gamma\gamma$-coincidence data and the decay of the isomeric state allowed

building a partial level scheme for ^{78}Cu. Spins and parities could be tentatively assigned for some of the states.

The experimental results were compared with large-scale MCSM calculations using the A3DA-m interaction and a valence space comprising the $1f_{7/2}$, $2p_{3/2}$, $1f_{5/2}$, $2p_{1/2}$, $1g_{9/2}$, and $2d_{5/2}$ orbitals for both protons and neutrons. The shell-model calculations show a remarkable agreement with the experimental results. Combining the experimental results with the calculations, it was possible to interpret the low-lying states in terms of spin multiplets arising from the coupling of an odd proton in either the $\pi 1f_{5/2}$ or $\pi 2p_{3/2}$ orbital with an odd neutron in the $\nu 1g_{9/2}$, $\nu 2p_{1/2}$, or $\nu 2d_{5/2}$ orbital. The results confirm the previously observed crossing between the $\pi 2p_{3/2}$ and $\pi 1f_{5/2}$ orbitals. The interpretation of the isomeric state as based on the $\pi 1f_{5/2}$-$\nu 2d_{5/2}$ configuration provides information on the $N = 50$ shell gap. Because configurations are pure, it was possible to extract experimental two-body matrix elements for the $\pi 1f_{5/2}$-$\nu 1g_{9/2}^{-1}$ interaction, which represent important input for future shell-model calculations in the ^{78}Ni region. Extending the work to ^{80}Cu would represent an important step for investigating the proton-neutron interaction beyond ^{78}Ni.

ACKNOWLEDGMENTS

This work was carried out at the RIBF operated by RIKEN Nishina Center, RIKEN and CNS, University of Tokyo. This work was partially supported by KAKENHI (Grants No. 25247045, No. 23.01752, and No. 25800130). The authors acknowledge the EUROBALL Owners Committee for the loan of germanium detectors and the PreSpec Collaboration for the readout electronics of the cluster detectors. This work was partially supported by the Norwegian Research Council under project Contracts No. 240104, 262952, 263030, and 288061. The Monte Carlo shell-model calculations were performed on the K computer at RIKEN AICS (hp160211, hp170230, hp180179, hp190160). This work was supported in part by MEXT as "Priority Issue on Post-K Computer" (Elucidation of the Fundamental Laws and Evolution of the Universe) and as "Program for Promoting Researches on the Supercomputer Fugaku" (Simulation for basic science: from fundamental laws of particles to creation of nuclei) (hp200130) and JICFuS. Support from German BMBF Grant No. 05P19RDFN1 and No. 05P21RDFN1, from US DOE Grant No. DE-FG02-91ER-40609, from the National Research, Development and Innovation Fund of Hungary via Project No. K128947 and TKP2021-NKTA-42 is acknowledged. University of Brighton authors were supported by STFC Grant No. ST/J000132/1. This work was partially supported by Helmholtz Forschungsakademie Hessen für FAIR (HFHF), GSI Helmholtzzentrum für Schwerionenforschung, Campus Darmstadt, 64289 Darmstadt, Germany, and by Generalitat Valenciana, Conselleria de Innovación, Universidades, Ciencia y Sociedad Digital (CISEJI/2022/25).

[1] O. Sorlin and M.-G. Porquet, Prog. Part. Nucl. Phys. **61**, 602 (2008).
[2] T. Otsuka, A. Gade, O. Sorlin, T. Suzuki, and Y. Utsuno, Rev. Mod. Phys. **92**, 015002 (2020).
[3] R. Taniuchi, C. Santamaria, P. Doornenbal, A. Obertelli, K. Yoneda, G. Authelet, H. Baba, D. Calvet, F. Château, A. Corsi, A. Delbart, J.-M. Gheller, A. Gillibert, J. D. Holt, T. Isobe, V. Lapoux, M. Matsushita, J. Menéndez, S. Momiyama, T. Motobayashi *et al.*, Nature (London) **569**, 53 (2019).
[4] Z. Y. Xu, S. Nishimura, G. Lorusso, F. Browne, P. Doornenbal, G. Gey, H.-S. Jung, Z. Li, M. Niikura, P.-A. Söderström, T. Sumikama, J. Taprogge, Z. Vajta, H. Watanabe, J. Wu, A. Yagi, K. Yoshinaga, H. Baba, S. Franchoo, T. Isobe *et al.*, Phys. Rev. Lett. **113**, 032505 (2014).
[5] A. Welker, N. A. S. Althubiti, D. Atanasov, K. Blaum, T. E. Cocolios, F. Herfurth, S. Kreim, D. Lunney, V. Manea, M. Mougeot, D. Neidherr, F. Nowacki, A. Poves, M. Rosenbusch, L. Schweikhard, F. Wienholtz, R. N. Wolf, and K. Zuber, Phys. Rev. Lett. **119**, 192502 (2017).
[6] K.-L. Kratz, H. Gabelmann, P. Möller, B. Pfeiffer, H. L. Ravn, A. Wöhr, and The ISOLDE Collaboration, Z. Phys. A **340**, 419 (1991).
[7] S. Nikas, G. M. Pinedo, and A. Sieverding, J. Phys.: Conf. Ser. **1668**, 012029 (2020).
[8] K. T. Flanagan, P. Vingerhoets, M. Avgoulea, J. Billowes, M. L. Bissell, K. Blaum, B. Cheal, M. De Rydt, V. N. Fedosseev, D. H. Forest, C. Geppert, U. Köster, M. Kowalska, J. Krämer, K. L. Kratz, A. Krieger, E. Mané, B. A. Marsh, T. Materna, L. Mathieu *et al.*, Phys. Rev. Lett. **103**, 142501 (2009).
[9] E. Sahin, F. L. Bello Garrote, Y. Tsunoda, T. Otsuka, G. de Angelis, A. Görgen, M. Niikura, S. Nishimura, Z. Y. Xu, H. Baba, F. Browne, M.-C. Delattre, P. Doornenbal, S. Franchoo, G. Gey, K. Hadyńska-Klk, T. Isobe, P. R. John, H. S. Jung, I. Kojouharov *et al.*, Phys. Rev. Lett. **118**, 242502 (2017).
[10] C. Petrone, J. M. Daugas, G. S. Simpson, M. Stanoiu, C. Plaisir, T. Faul, C. Borcea, R. Borcea, L. Cáceres, S. Calinescu, R. Chevrier, L. Gaudefroy, G. Georgiev, G. Gey, O. Kamalou, F. Negoita, F. Rotaru, O. Sorlin, and J. C. Thomas, Phys. Rev. C **94**, 024319 (2016).
[11] L. Olivier, S. Franchoo, M. Niikura, Z. Vajta, D. Sohler, P. Doornenbal, A. Obertelli, Y. Tsunoda, T. Otsuka, G. Authelet, H. Baba, D. Calvet, F. Château, A. Corsi, A. Delbart, J.-M. Gheller, A. Gillibert, T. Isobe, V. Lapoux, M. Matsushita *et al.*, Phys. Rev. Lett. **119**, 192501 (2017).
[12] T. Otsuka, T. Suzuki, R. Fujimoto, H. Grawe, and Y. Akaishi, Phys. Rev. Lett. **95**, 232502 (2005).
[13] J. Van Roosbroeck, H. De Witte, M. Gorska, M. Huyse, K. Kruglov, D. Pauwels, J.-C. Thomas, K. Van de Vel, P. Van Duppen, S. Franchoo, J. Cederkall, V. N. Fedoseyev, H. Fynbo, U. Georg, O. Jonsson, U. Köster, L. Weissman, W. F. Mueller, V. I. Mishin, D. Fedorov *et al.*, Phys. Rev. C **71**, 054307 (2005).
[14] V. Paar, Nucl. Phys. A **331**, 16 (1979).
[15] N. Shimizu, T. Abe, Y. Tsunoda, Y. Utsuno, T. Yoshida, T. Mizusaki, M. Honma, and T. Otsuka, Prog. Theor. Exp. Phys. **2012**, 01A205 (2012).
[16] Y. Tsunoda, T. Otsuka, N. Shimizu, M. Honma, and Y. Utsuno, Phys. Rev. C **89**, 031301(R) (2014).

[17] K. Langanke, G. Martínez-Pinedo, J. M. Sampaio, D. J. Dean, W. R. Hix, O. E. B. Messer, A. Mezzacappa, M. Liebendörfer, H.-T. Janka, and M. Rampp, Phys. Rev. Lett. **90**, 241102 (2003).

[18] R. P. de Groote, J. Billowes, C. L. Binnersley, M. L. Bissell, T. E. Cocolios, T. Day Goodacre, G. J. Farooq-Smith, D. V. Fedorov, K. T. Flanagan, S. Franchoo, R. F. Garcia Ruiz, A. Koszorús, K. M. Lynch, G. Neyens, F. Nowacki, T. Otsuka, S. Rothe, H. H. Stroke, Y. Tsunoda, A. R. Vernon *et al.*, Phys. Rev. C **96**, 041302(R) (2017).

[19] P.-A. Söderström, S. Nishimura, P. Doornenbal, G. Lorusso, T. Sumikama, H. Watanabe, Z. Xu, H. Baba, F. Browne, S. Go, G. Gey, T. Isobe, H.-S. Jung, G. Kim, Y.-K. Kim, I. Kojouharov, N. Kurz, Y. Kwon, Z. Li, K. Moschner *et al.*, Nucl. Instrum. Methods Phys. Res., Sect. B **317**, 649 (2013).

[20] N. Fukuda, T. Kubo, T. Ohnishi, N. Inabe, H. Takeda, D. Kameda, and H. Suzuki, Nucl. Instrum. Methods Phys. Res., Sect. B **317**, 323 (2013).

[21] T. Kubo, D. Kameda, H. Suzuki, N. Fukuda, H. Takeda, Y. Yanagisawa, M. Ohtake, K. Kusaka, K. Yoshida, N. Inabe, T. Ohnishi, A. Yoshida, K. Tanaka, and Y. Mizoi, Prog. Theor. Exp. Phys. **2012**, 03C003 (2012).

[22] S. Nishimura, Prog. Theor. Exp. Phys. **2012**, 03C006 (2012).

[23] M. Wang, W. Huang, F. Kondev, G. Audi, and S. Naimi, Chin. Phys. C **45**, 030003 (2021).

[24] A. Tolosa Delgado, Ph.D. thesis, U. Valencia (main), 2020 (unpublished).

[25] C. J. Gross, J. A. Winger, S. V. Ilyushkin, K. P. Rykaczewski, S. N. Liddick, I. G. Darby, R. K. Grzywacz, C. R. Bingham, D. Shapira, C. Mazzocchi, S. Padgett, M. M. Rajabali, L. Cartegni, E. F. Zganjar, A. Piechaczek, J. C. Batchelder, J. H. Hamilton, C. T. Goodin, A. Korgul, and W. Królas, Acta Phys. Pol. B **40**, 447 (2009).

[26] A. Korgul, K. P. Rykaczewski, J. A. Winger, S. V. Ilyushkin, C. J. Gross, J. C. Batchelder, C. R. Bingham, I. N. Borzov, C. Goodin, R. Grzywacz, J. H. Hamilton, W. Królas, S. N. Liddick, C. Mazzocchi, C. Nelson, F. Nowacki, S. Padgett, A. Piechaczek, M. M. Rajabali, D. Shapira *et al.*, Phys. Rev. C **86**, 024307 (2012).

[27] T. Kibédi, T. Burrows, M. Trzhaskovskaya, P. Davidson, and C. Nestor, Nucl. Instrum. Methods Phys. Res., Sect. A **589**, 202 (2008).

[28] F. L. Bello Garrote, E. Sahin, Y. Tsunoda, T. Otsuka, A. Görgen, M. Niikura, S. Nishimura, G. de Angelis, G. Benzoni, A. I. Morales, V. Modamio, Z. Y. Xu, H. Baba, F. Browne, A. M. Bruce, S. Ceruti, F. C. L. Crespi, R. Daido, M.-C. Delattre, P. Doornenbal *et al.*, Phys. Rev. C **102**, 034314 (2020).

[29] S. Giraud, L. Canete, B. Bastin, A. Kankainen, A. Fantina, F. Gulminelli, P. Ascher, T. Eronen, V. Girard-Alcindor, A. Jokinen, A. Khanam, I. Moore, D. Nesterenko, F. de Oliveira Santos, H. Penttilä, C. Petrone, I. Pohjalainen, A. De Roubin, V. Rubchenya, M. Vilen *et al.*, Phys. Lett. B **833**, 137309 (2022).

[30] S. P. Pandya, Phys. Rev. **103**, 956 (1956).